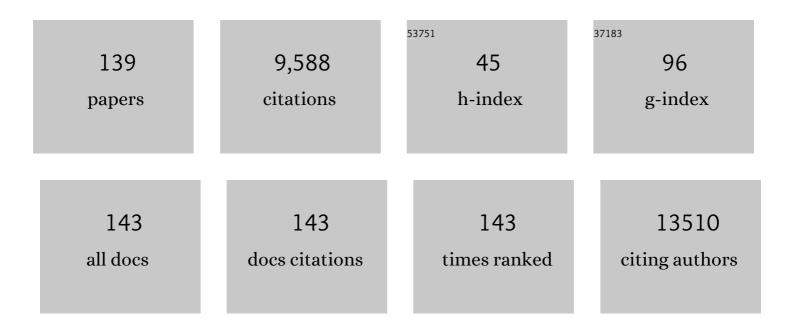
Matthew F Chisholm

List of Publications by Year in descending order

Source: https://exaly.com/author-pdf/7442421/publications.pdf Version: 2024-02-01



#	Article	IF	CITATIONS
1	Atom-by-atom structural and chemical analysis by annular dark-field electron microscopy. Nature, 2010, 464, 571-574.	13.7	1,138
2	Strong polarization enhancement in asymmetric three-component ferroelectric superlattices. Nature, 2005, 433, 395-399.	13.7	627
3	PdSe ₂ : Pentagonal Two-Dimensional Layers with High Air Stability for Electronics. Journal of the American Chemical Society, 2017, 139, 14090-14097.	6.6	509
4	Atomically Dispersed Transition Metals on Carbon Nanotubes with Ultrahigh Loading for Selective Electrochemical Carbon Dioxide Reduction. Advanced Materials, 2018, 30, e1706287.	11.1	459
5	Reversible redox reactions in an epitaxially stabilized SrCoOx oxygen sponge. Nature Materials, 2013, 12, 1057-1063.	13.3	349
6	Defectâ€Tailoring Mediated Electron–Hole Separation in Singleâ€Unitâ€Cell Bi ₃ O ₄ Br Nanosheets for Boosting Photocatalytic Hydrogen Evolution and Nitrogen Fixation. Advanced Materials, 2019, 31, e1807576.	11.1	311
7	Spatially controlled doping of two-dimensional SnS2 through intercalation for electronics. Nature Nanotechnology, 2018, 13, 294-299.	15.6	269
8	Catalytically active single-atom niobium in graphitic layers. Nature Communications, 2013, 4, 1924.	5.8	261
9	Bismuth-induced embrittlement of copper grain boundaries. Nature Materials, 2004, 3, 621-626.	13.3	242
10	Wide bandgap tunability in complex transition metal oxides by site-specific substitution. Nature Communications, 2012, 3, 689.	5.8	237
11	Growth and microstructure of superconducting YBa2Cu3Ox single crystals. Journal of Crystal Growth, 1987, 85, 593-598.	0.7	219
12	MATERIALS CHARACTERIZATION IN THE ABERRATION-CORRECTED SCANNING TRANSMISSION ELECTRON MICROSCOPE. Annual Review of Materials Research, 2005, 35, 539-569.	4.3	188
13	Growth and relaxation mechanisms of YBa2Cu3O7â ^{~°} x films. Physica C: Superconductivity and Its Applications, 1992, 202, 1-11.	0.6	176
14	Gentle STEM: ADF imaging and EELS at low primary energies. Ultramicroscopy, 2010, 110, 935-945.	0.8	174
15	Solid-state synthesis of ordered mesoporous carbon catalysts via a mechanochemical assembly through coordination cross-linking. Nature Communications, 2017, 8, 15020.	5.8	164
16	Rheniumâ€Ðoped and Stabilized MoS ₂ Atomic Layers with Basalâ€Plane Catalytic Activity. Advanced Materials, 2018, 30, e1803477.	11.1	164
17	Dislocations in Complex Materials. Science, 2005, 307, 701-703.	6.0	156
18	The atomic origins of reduced critical currents at [001] tilt grain boundaries in YBa2Cu3O7â~'δ thin films. Physica C: Superconductivity and Its Applications, 1998, 294, 183-193.	0.6	150

#	Article	IF	CITATIONS
19	Suppressed Dependence of Polarization on Epitaxial Strain in Highly Polar Ferroelectrics. Physical Review Letters, 2007, 98, 217602.	2.9	146
20	Atomic-Scale Compensation Phenomena at Polar Interfaces. Physical Review Letters, 2010, 105, 197602.	2.9	146
21	Crown ethers in graphene. Nature Communications, 2014, 5, 5389.	5.8	142
22	Topological Defects: Origin of Nanopores and Enhanced Adsorption Performance in Nanoporous Carbon. Small, 2012, 8, 3283-3288.	5.2	139
23	Direct observation of dislocation dissociation and Suzuki segregation in a Mg–Zn–Y alloy by aberration-corrected scanning transmission electron microscopy. Acta Materialia, 2013, 61, 350-359.	3.8	126
24	lonization-induced annealing of pre-existing defects in silicon carbide. Nature Communications, 2015, 6, 8049.	5.8	116
25	Engineering Ferroelectric Hf _{0.5} Zr _{0.5} O ₂ Thin Films by Epitaxial Stress. ACS Applied Electronic Materials, 2019, 1, 1449-1457.	2.0	105
26	Single-crystal high entropy perovskite oxide epitaxial films. Physical Review Materials, 2018, 2, .	0.9	102
27	Correlation between hole depletion and atomic structure at high angle grain boundaries in YBa2Cu3O7â~δ. Physica C: Superconductivity and Its Applications, 1993, 212, 185-190.	0.6	99
28	Synergy of elastic and inelastic energy loss on ion track formation in SrTiO3. Scientific Reports, 2015, 5, 7726.	1.6	98
29	Orienting Oxygen Vacancies for Fast Catalytic Reaction. Advanced Materials, 2013, 25, 6459-6463.	11.1	96
30	The observation of square ice in graphene questioned. Nature, 2015, 528, E1-E2.	13.7	95
31	The effect of growth parameters on the intrinsic properties of large-area single layer graphene grown by chemical vapor deposition on Cu. Carbon, 2012, 50, 134-141.	5.4	92
32	Effects of Surface Terminations of 2D Bi ₂ WO ₆ on Photocatalytic Hydrogen Evolution from Water Splitting. ACS Applied Materials & Interfaces, 2020, 12, 20067-20074.	4.0	78
33	Stabilization of graphene nanopore. Proceedings of the National Academy of Sciences of the United States of America, 2014, 111, 7522-7526.	3.3	76
34	Thermal stability of epitaxial SrRuO3 films as a function of oxygen pressure. Applied Physics Letters, 2004, 84, 4107-4109.	1.5	71
35	The synergistic role of Mn and Zr/Ti in producing Î,′/L12 co-precipitates in Al-Cu alloys. Acta Materialia, 2020, 194, 577-586.	3.8	71
36	Observation of structural units at symmetric [001] tilt boundaries in SrTiO3. Journal of Materials Science, 1995, 2, 397.	1.2	70

#	Article	IF	CITATIONS
37	The structure of ã€^ <i>c</i> + <i>a</i> 〉 type dislocation loops in magnesium. Philosophical Magaz Letters, 2014, 94, 377-386.	ine _{0.5}	70
38	Atomic-resolution spectroscopic imaging: past, present and future. Journal of Electron Microscopy, 2009, 58, 87-97.	0.9	66
39	Oxidation Resistance of Reactive Atoms in Graphene. Nano Letters, 2012, 12, 4651-4655.	4.5	64
40	An electron microscopy study of dislocation structures in Mg single crystals compressed along [0 0 0 1] at room temperature. Philosophical Magazine, 2015, 95, 3910-3932.	0.7	61
41	Domain-Matching Epitaxy of Ferroelectric Hf _{0.5} Zr _{0.5} O ₂ (111) on La _{2/3} Sr _{1/3} MnO ₃ (001). Crystal Growth and Design, 2020, 20, 3801-3806.	1.4	60
42	Surface Reorganization Leads to Enhanced Photocatalytic Activity in Defective BiOCl. Chemistry of Materials, 2018, 30, 5128-5136.	3.2	55
43	Role of crystal defects on brittleness of C15 Cr2Nb Laves phase. Acta Materialia, 2012, 60, 2637-2646.	3.8	53
44	Ambipolar ferromagnetism by electrostatic doping of a manganite. Nature Communications, 2018, 9, 1897.	5.8	51
45	Atomic Layer Engineering of Perovskite Oxides for Chemically Sharp Heterointerfaces. Advanced Materials, 2012, 24, 6423-6428.	11.1	49
46	Controlling Reaction Selectivity through the Surface Termination of Perovskite Catalysts. Angewandte Chemie - International Edition, 2017, 56, 9820-9824.	7.2	47
47	Protecting the Nanoscale Properties of Ag Nanowires with a Solution-Grown SnO ₂ Monolayer as Corrosion Inhibitor. Journal of the American Chemical Society, 2019, 141, 13977-13986.	6.6	45
48	Ultrathin GaN quantum disk nanowire LEDs with sub-250 nm electroluminescence. Nanoscale, 2016, 8, 8024-8032.	2.8	44
49	Unsupported single-atom-thick copper oxide monolayers. 2D Materials, 2017, 4, 011001.	2.0	44
50	Unraveling Ferroelectric Polarization and Ionic Contributions to Electroresistance in Epitaxial Hf _{0.5} Zr _{0.5} O ₂ Tunnel Junctions. Advanced Electronic Materials, 2020, 6, 1900852.	2.6	44
51	SUPERNOVA SHOCK-WAVE-INDUCED CO-FORMATION OF GLASSY CARBON AND NANODIAMOND. Astrophysical Journal Letters, 2011, 738, L27.	3.0	42
52	Misfit accommodation in oxide thin film heterostructures. Acta Materialia, 2013, 61, 2725-2733.	3.8	42
53	Persistent Electrochemical Performance in Epitaxial VO ₂ (B). Nano Letters, 2017, 17, 2229-2233.	4.5	41
54	Dislocation-driven growth of two-dimensional lateral quantum-well superlattices. Science Advances, 2018, 4, eaap9096.	4.7	38

#	Article	IF	CITATIONS
55	Direct Observation of Atomic Dynamics and Silicon Doping at a Topological Defect in Graphene. Angewandte Chemie - International Edition, 2014, 53, 8908-8912.	7.2	37
56	Atomic-scale structure and chemistry of ceramic/metal interfaces—I. Atomic structure of {222} MgO/Cu (Ag) interfaces. Acta Materialia, 1999, 47, 3939-3951.	3.8	36
57	Concurrent Synthesis of Highâ€Performance Monolayer Transition Metal Disulfides. Advanced Functional Materials, 2017, 27, 1605896.	7.8	35
58	Fast ion conductivity in strained defect-fluorite structure created by ion tracks in Gd2Ti2O7. Scientific Reports, 2015, 5, 16297.	1.6	33
59	Tungsten Diselenide Patterning and Nanoribbon Formation by Gasâ€Assisted Focusedâ€Heliumâ€Ionâ€Beamâ€Induced Etching. Small Methods, 2017, 1, 1600060.	4.6	33
60	Precipitation of binary quasicrystals along dislocations. Nature Communications, 2018, 9, 809.	5.8	30
61	Spatial Resolution and Information Transfer in Scanning Transmission Electron Microscopy. Microscopy and Microanalysis, 2008, 14, 36-47.	0.2	27
62	Colossal photon bunching in quasiparticle-mediated nanodiamond cathodoluminescence. Physical Review B, 2018, 97, .	1.1	26
63	Atomic-scale manipulation of potential barriers at SrTiO3 grain boundaries. Applied Physics Letters, 2005, 87, 121917.	1.5	25
64	Scanning transmission electron microscopy: Albert Crewe's vision and beyond. Ultramicroscopy, 2012, 123, 90-98.	0.8	25
65	Pulsed-laser epitaxy of metallic delafossite PdCrO2 films. APL Materials, 2020, 8, .	2.2	25
66	Metal–insulator transition tuned by oxygen vacancy migration across TiO2/VO2 interface. Scientific Reports, 2020, 10, 18554.	1.6	24
67	Low-Temperature Resistance Anomaly atSrTiO3Grain Boundaries: Evidence for an Interface-Induced Phase Transition. Physical Review Letters, 2005, 95, 197601.	2.9	23
68	Symmetryâ€Driven Atomic Rearrangement at a Brownmillerite–Perovskite Interface. Advanced Electronic Materials, 2016, 2, 1500201.	2.6	23
69	Control of Polar Orientation and Lattice Strain in Epitaxial BaTiO ₃ Films on Silicon. ACS Applied Materials & Interfaces, 2018, 10, 25529-25535.	4.0	23
70	Direct Cation Exchange in Monolayer <mml:math <br="" xmlns:mml="http://www.w3.org/1998/Math/MathML">display="inline"><mml:mrow><mml:msub><mml:mrow><mml:mi>MoS</mml:mi></mml:mrow><mml:mn>2< via Recombination-Enhanced Migration. Physical Review Letters, 2019, 122, 106101.</mml:mn></mml:msub></mml:mrow></mml:math>	/mml ærø n> </td <td>/mn2l1msub><</td>	/mn 2l1 msub><
71	Rotational polarization nanotopologies in BaTiO ₃ /SrTiO ₃ superlattices. Nanoscale, 2019, 11, 21275-21283.	2.8	21
72	Role of shell composition and morphology in achieving single-emitter photostability for	1.2	20

Role of shell composition and morphology in achieving single-emitter photostability for green-emitting "giant―quantum dots. Journal of Chemical Physics, 2020, 152, 124713. 72 1.2

#	Article	IF	CITATIONS
73	Chapter 9 Materials Applications of Aberration-Corrected Scanning Transmission Electron Microscopy. Advances in Imaging and Electron Physics, 2008, , 327-384.	0.1	19
74	Controlling Reaction Selectivity through the Surface Termination of Perovskite Catalysts. Angewandte Chemie, 2017, 129, 9952-9956.	1.6	19
75	One-Pot Pyrolysis Method to Fabricate Carbon Nanotube Supported Ni Single-Atom Catalysts with Ultrahigh Loading. ACS Applied Energy Materials, 0, , .	2.5	19
76	Z-Contrast Imaging of Grain-Boundary Core Structures in Semiconductors. MRS Bulletin, 1997, 22, 53-57.	1.7	18
77	Nanoscale self-templating for oxide epitaxy with large symmetry mismatch. Scientific Reports, 2016, 6, 38168.	1.6	18
78	Quantum critical behavior in the asymptotic limit of high disorder in the medium entropy alloy NiCoCr0.8. Npj Quantum Materials, 2017, 2, .	1.8	18
79	Atomic structures of interfacial solute gateways to Î,′ precipitates in Al-Cu alloys. Acta Materialia, 2021, 212, 116891.	3.8	18
80	The Electronic Structure of Pristine and Doped (100) Tilt Grain Boundaries in SrTiO3. Journal of Materials Science, 2000, 8, 199-208.	1.2	16
81	Effects of Negative-Bias-Temperature-Instability on Low-Frequency Noise in SiGe \${p}\$ MOSFETs. IEEE Transactions on Device and Materials Reliability, 2016, 16, 541-548.	1.5	16
82	Effect of indium alloying on the charge carrier dynamics of thick-shell InP/ZnSe quantum dots. Journal of Chemical Physics, 2020, 152, 161104.	1.2	16
83	A combined experimental and theoretical approach to grain boundary structure and segregation. Physica B: Condensed Matter, 1999, 273-274, 453-457.	1.3	15
84	Spontaneous cationic ordering in chemical-solution-grown La2CoMnO6 double perovskite thin films. NPG Asia Materials, 2019, 11, .	3.8	15
85	Strain-Induced Atomic-Scale Building Blocks for Ferromagnetism in Epitaxial LaCoO ₃ . Nano Letters, 2021, 21, 4006-4012.	4.5	15
86	Insights on dramatic radial fluctuations in track formation by energetic ions. Scientific Reports, 2016, 6, 27196.	1.6	14
87	Monoâ€Atomic Fe Centers in Nitrogen/Carbon Monolayers for Liquidâ€Phase Selective Oxidation Reaction. ChemCatChem, 2018, 10, 3539-3545.	1.8	14
88	Atomic Structure and Properties of Extended Defects in Silicon. Solid State Phenomena, 1999, 67-68, 3-14.	0.3	13
89	New insights on ion track morphology in pyrochlores by aberration corrected scanning transmission electron microscopy. Journal of Materials Research, 2017, 32, 928-935.	1.2	13
90	{001} faults in B2 Fe-40 at.% Al-0.7 at.% C-0.5 at.% B. Philosophical Magazine Letters, 1998, 78, 349-355.	0.5	11

ARTICLE IF CITATIONS Structures of pure and Ca-segregated MgO (001) surfaces. Surface Science, 1999, 442, 251-255. Title is missing!. , 2000, 4, 279-287. 92 11 Intrinsic interfacial van der Waals monolayers and their effect on the high-temperature superconductor <mml:math xmlns:mml="http://www.w3.org/1998/Math/MathML"><mml:msub><mml:mrow><mml:mi>FeSe</mml:mi><mml:mo><m Physical Review B, 2019, 100. Detection of defects in atomic-resolution images of materials using cycle analysis. Advanced 94 4.0 11 Structural and Chemical Imaging, 2020, 6, . Direct observation of solute interstitials and their clusters in Mg alloys. Materials Characterization, 1.9 2017, 128, 226-231. A Combined Experimental and Theoretical Approach to Atomic Structure and Segregation at Ceramic 96 2.8 9 Interfaces. Journal of the European Ceramic Society, 1999, 19, 2211-2216. Activation Energies for Oxide- and Interface-Trap Charge Generation Due to Negative-Bias Temperature Stress of Si-Capped SiGe-pMOSFETs. IEEE Transactions on Device and Materials Reliability, 2015, 15, 1.5 352-358. Magnetic Ordering in Sr3YCo4O10+x. Scientific Reports, 2016, 6, 19762. 98 1.6 9 Vacancy Formation and Vacancy-Induced Structural Transformation in Si Grain Boundaries. Materials 0.3 Science Forum, 1998, 294-296, 161-164. 100 Atomic-Resolution STEM at Low Primary Energies., 2011, , 615-658. 8 Singleâ€Atom Catalysts: Atomically Dispersed Transition Metals on Carbon Nanotubes with Ultrahigh Loading for Selective Electrochemical Carbon Dioxide Reduction (Adv. Mater. 13/2018). Advanced 11.1 Materials, 2018, 30, 1870088. 102 Templated epitaxy of TiO2(B) on a perovskite. Applied Physics Letters, 2020, 117, . 1.5 8 Interfacial stabilization for epitaxial CuCrO2 delafossites. Scientific Reports, 2020, 10, 11375. 1.6 Total lonizing Dose Effects on Ge Channel <formula formulatype="inline"><tex Notation="TeX">\$p\$</tex></formula>FETs with Raised <formula formulatype="inline"><tex Notation="TeX">\${m Si}_{0.55}{m Ge}_{0.45}\$</tex></formula> Source/Drain. IEEE Transactions on Nuclear Science, 2015, 62, 104 1.2 7 2412-2416. Sculpting Nanoscale Functional Channels in Complex Oxides Using Energetic Ions and Electrons. ACS Applied Materials & amp; Interfaces, 2018, 10, 16731-16738. Investigating phase transitions from local crystallographic analysis based on statistical learning of 106 5.5 7 atomic environments in 2D MoS2-ReS2. Applied Physics Reviews, 2021, 8, 011409. Twin-Domain Formation in Epitaxial Triangular Lattice Delafossites. ACS Applied Materials & amp; 4.0 Interfaces, 2021, 13, 22059-22064.

MATTHEW F CHISHOLM

6

108Nonequilibrium Synthesis of Highly Porous Singleâ€Crystalline Oxide Nanostructures. Advanced1.9108Materials Interfaces, 2017, 4, 1601034.1.9

#	Article	IF	CITATIONS
109	Kinetically Controlled Fabrication of Singleâ€Crystalline TiO 2 Nanobrush Architectures with High Energy {001} Facets. Advanced Science, 2017, 4, 1700045.	5.6	5
110	Atomic-scale processes revealing dynamic twin boundary strengthening mechanisms in face-centered cubic materials. Scripta Materialia, 2012, 67, 911-914.	2.6	4
111	Tuning High Order Geometric Aberrations in Quadrupole-Octupole Correctors. Microscopy and Microanalysis, 2014, 20, 928-929.	0.2	4
112	Amorphization and recrystallization of YBa2Cu3O7â x by ion implantation and annealing. Nuclear Instruments & Methods in Physics Research B, 1993, 79, 641-644.	0.6	3
113	Letter to the Editor: Limitations to the Measurement of Oxygen Concentrations by HRTEM Imposed by Surface Roughness. Microscopy and Microanalysis, 2005, 11, 111-113.	0.2	3
114	Nanoporous Carbon: Topological Defects: Origin of Nanopores and Enhanced Adsorption Performance in Nanoporous Carbon (Small 21/2012). Small, 2012, 8, 3282-3282.	5.2	3
115	Effective reduction of <mml:math xmlns:mml="http://www.w3.org/1998/Math/MathML"><mml:msub><mml:mi>PdCoO</mml:mi><mml:mn>2thin films via hydrogenation and sign tunable anomalous Hall effect. Physical Review Materials, 2021, 5</mml:mn></mml:msub></mml:math 	ml:mn> </td <td>mmgl:msub><!--</td--></td>	mmgl:msub> </td
116	High Resolution Z-Contrast Observation of GaAs/Si Hetero-Interfaces through Scanning Transmission Electron Microscope. Japanese Journal of Applied Physics, 1992, 31, L1788-L1790.	0.8	2
117	Publisher's Note: Suppressed Dependence of Polarization on Epitaxial Strain in Highly Polar Ferroelectrics [Phys. Rev. Lett.98, 217602 (2007)]. Physical Review Letters, 2007, 98, .	2.9	2
118	Anti-Site Defects in Perovskite YAlO3:Ce Using Aberration-Corrected STEM. Microscopy and Microanalysis, 2014, 20, 132-133.	0.2	2
119	Two-dimensional metamaterials for epitaxial heterostructures. Current Opinion in Solid State and Materials Science, 2014, 18, 46-52.	5.6	2
120	Atomic resolution chemical analysis. Advanced Materials, 1994, 6, 328-331.	11.1	1
121	Stabilization of Nanopores in Graphene. Microscopy and Microanalysis, 2014, 20, 1732-1733.	0.2	1
122	Functionalization of Graphene. Microscopy and Microanalysis, 2015, 21, 737-738.	0.2	1
123	Formation of Single-atom-thick Copper Oxide Monolayers. Microscopy and Microanalysis, 2017, 23, 1684-1685.	0.2	1
124	Oxide Epitaxy with Large Symmetry Mismatch: Bronze-phase VO2 on SrTiO3. Microscopy and Microanalysis, 2017, 23, 1580-1581.	0.2	1
125	Thermodynamics of order and randomness in dopant distributions inferred from atomically resolved imaging. Npj Computational Materials, 2021, 7, .	3.5	1
126	Complex Diffusive Processes in Silicon. Defect and Diffusion Forum, 1997, 143-147, 971-978.	0.4	0

#	Article	IF	CITATIONS
127	Atomic scale investigations of ferroelectricity in perovskite thin films. , 2008, , .		0
128	Nanoengineering: Atomic Layer Engineering of Perovskite Oxides for Chemically Sharp Heterointerfaces (Adv. Mater. 48/2012). Advanced Materials, 2012, 24, 6422-6422.	11.1	0
129	Direct Observation of Plasmonic Enhancement of Emission in Ag-nanoparticle-decorated ZnO nanostructures. Microscopy and Microanalysis, 2015, 21, 2389-2390.	0.2	0
130	Probing Plasmons in Three Dimensions within Random Morphology Nanostructures. Microscopy and Microanalysis, 2015, 21, 1683-1684.	0.2	0
131	Inversion of STEM EELS Data to Obtain Site Occupancy and Near Edge Structure. Microscopy and Microanalysis, 2015, 21, 2251-2252.	0.2	0
132	Pushing the Limits of Cathodoluminescence Signal Detection: Analyzing 2D Materials. Microscopy and Microanalysis, 2015, 21, 2049-2050.	0.2	0
133	Atomic Resolution STEM-EELS Study of Transition Electronic Localization State Induced by Strain. Microscopy and Microanalysis, 2015, 21, 617-618.	0.2	0
134	Observing Nanoscale Orbital Angular Momentum in Plasmon Vortices with Cathodoluminescence. Microscopy and Microanalysis, 2017, 23, 1694-1695.	0.2	0
135	Quantification of Low Voltage Images of 2-dimensional Materials in Aberration Corrected Scanning Transmission Electron Microscopy Microscopy and Microanalysis, 2017, 23, 464-465.	0.2	0
136	Exchange of Re and Mo atoms in MoS2 driven by Scanning Transmission Electron Microscopy. Microscopy and Microanalysis, 2017, 23, 1702-1703.	0.2	0
137	Mapping Giant Oscillator Excitons in Semiconducting Nano Wires. Microscopy and Microanalysis, 2017, 23, 374-375.	0.2	0
138	Dislocation-Driven Growth of Two-Dimensional Lateral Quantum Well Superlattices. Microscopy and Microanalysis, 2018, 24, 88-89.	0.2	0
139	Determination of rutile transition metal oxide (110) surface terminations by scanning tunneling microscopy contrast reversal. Physical Review B, 2021, 103, .	1.1	0